Atmospheric
Measurement
Techniques
Discussions

Systematic Comparison of Vectorial Spherical Radiative Transfer Models in Limb Scattering Geometry

Daniel Zawada[1], Ghislain Franssens[2], Robert Loughman[3], Antti Mikkonen[4], Alexei Rozanov[5], Claudia Emde[6], Adam Bourassa[1], Seth Dueck[1], Hannakaisa Lindqvist[4], Didier Ramon[7], Vladimir Rozanov[5], Emmanuel Dekemper[2], Erkki Kyrölä[4], John P. Burrows[5], Didier Fussen[2], and Doug Degenstein[1]

[1]Institute of Space and Atmospheric Studies, University of Saskatchewan, Saskatchewan, Canada
[2]Royal Belgian Institute for Space Aeronomy, Brussels, Belgium
[3]Department of Atmospheric and Planetary Sciences, Hampton University, Hampton, Virginia, USA
[4]Finnish Meteorological Institute, Helsinki, Finland
[5]Institute of Environmental Physics, University of Bremen, Bremen, Germany
[6]Meteorological Institute, Ludwig-Maximilians-University, Munich, Germany
[7]HYGEOS, Lille, France

Correspondence: Daniel Zawada (daniel.zawada@usask.ca)

Abstract. A comprehensive inter-comparison of seven radiative transfer models in the limb scattering geometry has been performed. Every model is capable of accounting for polarisation within a fully spherical atmosphere. Three models (GSLS, SASKTRAN-HR, and SCIATRAN) are deterministic, and four models (MYSTIC, SASKTRAN-MC, Siro, and SMART-G) are statistical using the Monte Carlo technique. A wide variety of test cases encompassing different atmospheric conditions, solar geometries, wavelengths, tangent altitudes, and Lambertian surface reflectances have been defined and executed for every model. For the majority of conditions it was found that the models agree to better than 0.2 % in the single scatter test cases and better than 1 % in the multiple scatter scalar and vector test cases, with some larger differences noted at high values of surface reflectance in multiple scatter. For the first time in limb geometry, the effect of atmospheric refraction was compared among four models that support it (GSLS, SASKTRAN-HR, SCIATRAN, and SMART-G). Differences among most models in multiple scatter with refraction enabled was less than 1 %, with larger differences observed for some models. Overall the agreement among the models with and without refraction is better than has been previously reported in both scalar and vector modes.

1 Introduction

The limb scattering measurement technique involves viewing through the side, the limb, of the atmosphere while measuring scattered sunlight (see Fig. 1). Measurements are performed in the ultraviolet, visible, and near infrared spectral ranges where

scattering of solar irradiance is the dominant source of measured radiation. Scattering occurs through Rayleigh scattering from the background atmosphere, as well as potential contributions of scattering from larger particles such as stratospheric aerosols and clouds. The signal is also affected through absorption by atmospheric constituents, typically by molecules such as ozone

20 or nitrogen dioxide in the ultraviolet and visible. In the near and short wave infrared, absorption is dominated by water vapour, methane, carbon dioxide, and molecular oxygen.

Figure 1. The limb viewing geometry and definitions of solar zenith angle, solar azimuth angle, solar scattering angle, and tangent altitude. The tangent altitude and solar zenith angles are defined relative to the un-refracted tangent point. Figure adapted from Zawada et al. (2015).

Several satellite-based limb scattering instruments have flown in the past few decades. Notably, the Optical Spectrograph and InfraRed Imager System (OSIRIS, Llewellyn et al., 2004) was launched on-board the Swedish satellite Odin (Murtagh et al., 2002) in 2001, the SCanning Imaging Absorption SpectroMeter for Atmospheric CHartographY (SCIAMACHY, Bovensmann, 1999) instrument on-board Envisat in 2002, and the Ozone Mapping and Profiler Suite Limb Profiler (OMPS-LP, Flynn et al.,

25 2006) on-board Suomi-NPP in 2011. Two versions of the primarily solar occultation instrument the Stratospheric Aerosol and Gase Experiment (SAGE), SAGE III-M (Mauldin et al., 1998) on Meteor-3M in 2001, and SAGE III-ISS (Cisewski et al., 2014) on the International Space Station (ISS) in 2016, have capability to make limb scatter measurements. The stellar occultation instrument, Global Ozone Monitoring by Occultation of Stars (GOMOS, Kyrölä et al., 2004), is also capable of taking limb

30 scatter measurements. OMPS-LP is planned to be re-launched on-board the JPSS-2 satellite in 2022, and a new instrument, the Atmospheric Limb Tracker for Investigation of the Upcoming Stratosphere (ALTIUS, Fussen et al., 2019) is currently under development by the European Space Agency for a planned 2024 launch.

Vertical profiles of limb scattering spectra can be inverted to obtain distributions of atmospheric constituents with spectral absorption or scattering features. These include but are not limited to: stratospheric aerosol (Bourassa et al., 2007; Von Savigny

35 et al., 2015), ozone (Roth et al., 2007; Degenstein et al., 2009; Rault and Spurr, 2010; Arosio et al., 2018), nitrogen dioxide (Butz et al., 2006; Sioris et al., 2017), water vapor (Rozanov et al., 2011b), and bromine oxide (McLinden and Bourassa, 2010; Rozanov et al., 2011a). Inversion of these spectra requires a Radiative Transfer Model (RTM) capable of simulating

the observed radiance, including all relevant physical effects for the constituent of interest. The accuracy of the RTM directly influences the accuracy of the retrieved profile.

40   All of the aforementioned retrieval methods use RTMs operating in scalar mode, where only the intensity, I, is computed rather than the full Stokes vector of the observed radiance. This is known to be a good approximation when the instrument itself is designed to be polarization insensitive. While there do exist errors in the intensity from neglecting polarization (Mishchenko et al., 1994), they tend to cancel in various normalization schemes used by the retrieval (Loughman et al., 2005). However, ALTIUS as well as similar instrument concepts (Elash et al., 2017; Kozun et al., 2020), are designed to measure a linear
45   polarized signal rather than the raw intensity. For these instruments it is required to use an RTM that is capable of simulating the full Stokes vector.

Several studies have been performed which inter-compare the accuracy of polarized RTMs (e.g. Emde et al., 2015, 2018), however these have been focused on viewing angles of at most 80° (a viewing angle of 90° would be limb viewing). For viewing geometries other than limb and occultation it is common to use the plane parallel assumption, which is generally not
50   applicable in the limb geometry. The approximative spherical approach, where single scattered radiance is calculated using a spherical atmosphere and the multiple scatter signal is approximated with a plane-parallel model, has been shown to have systematic errors in the limb viewing geometry (Loughman et al., 2004; McLinden and Bourassa, 2010). Recently, Korkin et al. (2020) have extended some of these results to a fully spherical atmosphere, but the scope of the project was limited to scalar radiative transfer.

55   The most comprehensive previous inter-comparison focusing on the limb scattering geometry was performed by Loughman et al. (2004). The deterministic models Gauss-Seidel Limb Scattering (GSLS), CDI and CDIPI (Rozanov et al., 2001, which are solvers implemented in SCIATRAN), and the statistical models Siro (Oikarinen et al., 1999) and MCC++ (Postylyakov, 2004) were considered. It was found that the statistical models generally agree to within 1.5% in the total scattering case, while the deterministic spherical models, CDIPI and GSLS, agree with the statistical models at the 2–4% level. While comparison
60   of the full Stokes vector was included for models that supported it, it was not the primary goal of the study. The results of this study have been used in benchmarking newly developed RTMs, such as SASKTRAN (Bourassa et al., 2008), or to evaluate new updates or features of RTMs as was done for GSLS (Loughman et al., 2015).

This study serves to both update the state of inter-comparison of RTMs in limb scattering geometry and to improve on it in several ways. Firstly, all participating RTMs simulate polarization in the atmosphere and provide full Stokes vectors
65   which are compared, these results are of significant importance for the upcoming ALTIUS mission. Secondly, the treatment of stratospheric aerosols is updated to use Mie scattering solution rather than a Henyey-Greenstein phase function; the Mie scattering treatment is more representative of the current state of limb retrievals (e.g. Rieger et al., 2019; Malinina et al., 2019; Taha et al., 2020). In addition, simulations including atmospheric refraction are included for the first time.

Descriptions of each model is presented in Sec. 2, with Sec. 3 describing the set up of the test cases in detail. The results and
70   discussion of the comparisons can be found in Sec. 4 with final conclusions in Sec. 5.

2 Model Descriptions

Generally, modern RTMs include a variety of tools to aid in specifying the atmospheric state and the viewing geometry. These could be relatively simple things such as pre-computed climatologies of pressure, temperature, and ozone, or something more involved such as built-in Mie scattering code to calculate the optical properties of stratospheric aerosol particles of a given size distribution. However, the core purpose of every RTM is to solve the radiative transfer equation. Some models may contain several algorithms to do this and each one is called a *solver* or *engine*. In many cases, these solvers start from fundamentally different assumptions and have their own characteristic features. For example, the RTM SCIATRAN contains several solvers, however only one (Discrete Ordinates Method-Vector) is capable of simulating polarised radiances (Stokes vectors). Two engines are included in this study for SASKTRAN, SASKTRAN-HR and SASKTRAN-MC, which solve the radiative transfer problem in a successive orders and Monte Carlo (MC) methods respectively.

RTMs typically belong to one of two classes: statistical or deterministic. Statistical models solve the radiative transfer equation using Monte Carlo simulation of photon paths through the atmosphere, while deterministic models use discretisation, interpolation, and various simplifying assumptions. Statistical models are often easier to implement since less assumptions are made, however they usually are orders of magnitude slower computationally.

2.1 Deterministic Models

Deterministic models solve the Radiative Transfer Equation (RTE) using some form of numerical integration over the Line Of Sight (LOS) and by making various simplifying assumptions. The choice of how and which quantities are discretised can result in completely different methods being applied to solving the RTE.

These methods can further be classified according to how the sphericity of the atmosphere is handled when calculating the multiple scattered radiance field. Plane parallel models assume a flat Earth, and can therefore not be applied to simulate the limb viewing geometry. Pseudo-spherical models employ a plane parallel solution, but initialise the data in the RTE with the solar irradiance attenuated through a spherical atmosphere. Approximative spherical models trace the observer LOS through a spherical atmosphere, calculate the single scatter term spherically, and then use an approximately spherical multiple scatter source function (typically from one or more pseudo-spherical calculations, although the exact method may vary from model to model). Lastly, fully spherical models account for sphericity in all aspects of the calculation.

Some of these approximations have been shown to have significant, systematic effects on calculated radiances in the limb viewing geometry. Most notably, approximate spherical methods which use a single plane parallel solution have been shown to be systematically high (on the order of 5%) at higher tangent altitudes (McLinden and Bourassa, 2010). Similar differences were noted by Loughman et al. (2004) in comparing approximate spherical models with fully spherical statistical models.

2.1.1 GSLS

The Gauss-Seidel Limb Scattering (GSLS) RTM builds upon the techniques described by Herman et al. (1994, 1995) to simulate the vectorial radiance in a spherical atmosphere. Line of sight rays are traced through a fully spherical atmosphere,

integrating a fully spherical single scatter source function and an approximate multiple scatter source. The approximate multiple scatter source is calculated at a selected number of solar zenith angles using a pseudo-spherical calculation. The number of solar zenith angles the multiple scatter source function is calculated at depends on the solar geometry and is shown in Loughman et al. (2015). GSLS has support for atmospheric refraction and analytic computation of approximate weighting functions. A full description of GSLS can be found within Loughman et al. (2004, 2015).

GSLS has been used in several projects involving the retrieval of atmospheric constituents from limb scatter measurements. Most notably, GSLS is currently used as the RTM for the operational version of the OMPS-LP ozone and stratospheric aerosol data products (Rault and Loughman, 2013). The OMPS-LP stratospheric aerosol algorithm has also been applied to SCIA-MACHY measurements (Taha et al., 2011). GSLS was also used in experimental retrievals using limb scatter measurements from SAGE III-M (Rault, 2005).

2.1.2 SASKTRAN-HR

SASKTRAN is a fully spherical vector RTM originally developed at the University of Saskatchewan to process data from the Optical Spectrograph and InfraRed Imaging System (OSIRIS, Llewellyn et al., 2004) instrument. A full description of SASKTRAN can be found in Bourassa et al. (2008) and Zawada et al. (2015), and details on the polarised calculation in Dueck et al. (2017). SASKTRAN includes both a statistical (SASKTRAN-MC, see Sec. 2.2.2) and a deterministic method (SASKTRAN-HR) to solve the RTE. The deterministic approach employs the successive order of scattering technique. The technique has a physical interpretation where radiance incident from the sun directly is used to calculate the single scattered radiance. The single scatter radiance is then used to calculate the second order of scatter, and the process is iterated until convergence. Refractive effects can also optionally be included, approximate analytic weighting functions calculated, and two- and three-dimensional atmospheres can be handled. The primary application of SASKTRAN has been as the forward model for retrievals of ozone (Degenstein et al., 2009), stratospheric aerosols (Bourassa et al., 2007), and nitrogen dioxide (Sioris et al., 2017) from the OSIRIS instrument. However, SASKTRAN has also been used in a variety of projects unrelated to OSIRIS. SASKTRAN has been adapted to process limb retrievals from other instruments, including stratospheric aerosols from SCIAMACHY measurements (Rieger et al., 2018) and stratospheric ozone from OMPS-LP measurements (Zawada et al., 2018). SASKTRAN was also used to analyse data from an acousto-optical tuneable filter based instrument, the Aerosol Limb Imager (ALI, Elash et al. (2016)), which is conceptually similar to the VIS-NIR channel of ALTIUS.

SASKTRAN-HR has various options that control the accuracy of the solution, but the main one is the number of diffuse profiles, i.e. the number of discretizations used in solar zenith angle to compute the multiple scatter field. The model has been configured to use the number of diffuse profiles required to obtain approximately 0.2% accuracy as a function of solar conditions shown in Zawada et al. (2015).

2.1.3 SCIATRAN

The SCIATRAN software package provides tools for modelling radiative transfer processes in the ultraviolet to thermal infrared spectral range. A detailed review of available algorithms, selected comparisons, and applications is given by Rozanov et al.

Atmospheric
Measurement
Techniques
Discussions

Open Access

EGU

(2014). SCIATRAN contains databases (or code modules) of optical properties and climatologies, and a set of engines to solve the RTE. The only solver capable of simulating the vector radiance field is the Discrete Ordinates Method-Vector (DOM-V) solver. The DOM-V solver uses the discrete ordinates method to simulate the pseudo-spherical solution used to initialize the spherical integration.

140   In the limb viewing geometry SCIATRAN can operate in two modes, fully spherical and approximate spherical. In the approximate spherical mode, the single scatter radiance is calculated accounting for the full sphericity of the Earth, while the multiple scattered signal is approximated by several pseudo-spherical calculations. In fully spherical mode, the approximate spherical solution is iterated in a fully spherical geometry to account for sphericity effects. The comparisons shown use the fully spherical mode of SCIATRAN.

145   SCIATRAN accounts for refractive effects and calculates approximate weighting functions. SCIATRAN has been used in numerous applications spanning multiple research areas. One of SCIATRANs primary applications is its use as the forward model for SCIAMACHY limb scatter retrievals of including, but not limited to, ozone (Rozanov et al., 2007), water vapour (Rozanov et al., 2011b), and stratospheric aerosols (Von Savigny et al., 2015; Malinina et al., 2018). SCIATRAN has also been successfully used in the inversion of data products from the observations of other limb missions, including the retrievals of

150 stratospheric aerosol from OSIRIS measurements (Rieger et al., 2018), and ozone and stratospheric aerosol from OMPS-LP measurements (Arosio et al., 2018; Malinina et al., 2020).

2.2   Statistical Models

Statistical models use Monte Carlo (MC) simulation to solve the RTE. In spherical geometry, the most common technique is the so-called backward MC method, or adjoint method. Here, photons are traced, starting at the sensor, through the atmosphere

155 and towards the sun; this in contrast to the forward method, where photons originate at the source (Sun). Along the photon path, the choice of where the photon scatters and the direction of scattering are sampled based on the probability of a scatter event occurring. The final radiance, and associated precision, are estimated by analysing an ensemble of a large number of photons.

    The MC technique naturally has few assumptions which allows for easier implementation of new features. A primary exam-

160 ple of this is implementing atmospheric constituents that vary in three full dimensions, rather than only in altitude. It is also quite natural to handle the full sphericity of the atmosphere. Because of these reasons, statistical models are primarily used as benchmark models and to study new effects. Statistical models are typically orders of magnitude slower than deterministic models and are thus usually not used in operational retrieval methods. They also contain inherent random noise, driven by the number of photons used in the simulation, which may need to be considered depending on the application.

165   2.2.1   MYSTIC

The Monte carlo code for the phYSically correct Tracing of photons In Cloudy atmospheres (MYSTIC) model (Mayer, 2009; Emde et al., 2010) is a statistical, fully spherical, polarised RTM that is distributed as part of the libRadtran software package (Emde et al., 2016; Mayer and Kylling, 2005). Mystic is capable of simulating radiances, irradiances, heating rates, and actinic

Atmospheric
Measurement
Techniques
Discussions

Open Access

EGU

170 fluxes in the solar and thermal spectral ranges. While MYSTIC was originally designed for applications in three-dimensional cloudy atmospheres, it contains the full functionality necessary to simulate limb scattered radiances. In spherical mode, MYSTIC uses the backward MC method. MYSTIC contains specialised variance reduction methods for handling strongly peaked phase functions (Buras and Mayer, 2011), and is capable of simulating the effects of a fully three-dimensional atmosphere. (Emde and Mayer, 2007; Emde et al., 2017). High-spectral resolution radiances can be simulated efficiently using the ALIS (Absorption Lines Importance Sampling) method (Emde et al., 2011).

2.2.2 SASKTRAN-MC

175

The SASKTRAN RTM contains a MC mode (SASKTRAN-MC) based upon the Siro algorithm (Oikarinen et al., 1999). The primary purpose of SASKTRAN-MC is to serve as a benchmark for the SASKTRAN-HR model.

SASKTRAN-MC is fully polarised, spherical, and also uses the backward MC method. SASKTRAN-MC is capable of handling three-dimensional atmospheres and includes options to simulate the radiance to a specific precision level, rather than 180 specifying the absolute number of photons to simulate. For more details see Zawada et al. (2015) and Dueck et al. (2017).

2.2.3 Siro

Siro is a statistical, fully spherical, polarised, RTM developed at the Finnish Meteorological Institute, using the backward MC method (Oikarinen et al., 1999). Siro is capable of simulating radiances where the atmosphere varies three-dimensionally (not only in altitude). Siro is commonly used as a reference model for both studying limb scattered radiance and in comparisons with 185 other RTMs. Oikarinen et al. (1999) used Siro to demonstrate the importance of multiple scattering for limb scatter instruments, and to simulate the effects of a three-dimensionally varying reflective surface (Oikarinen, 2002). In Oikarinen (2001) the effect of polarization on limb scatter radiance was assessed in detail using Siro. Siro played a key role in the RTM inter-comparison study performed by Loughman et al. (2004) as one of the MC reference models.

2.2.4 SMART-G

190 SMART-G (Speed-up Monte-carlo Advanced Radiative Transfer code with GPU) is a radiative transfer solver for the coupled ocean-atmosphere system with a wavy interface (Ramon et al., 2019) or any surface spectral BRDF boundary condition. It is based on the MC technique, works in either plane-parallel or spherical-shell geometry, and accounts for polarization. The vector code is written in CUDA (Compute Unified Device Architecture) and runs on GPUs (Graphic Processing Units). Physical processes included in the current version of the code are elastic scattering, absorption, reflection, thermal emission, 195 and refraction.

The radiances at any level of the domain can be estimated using the local estimate variance reduction method (Marchuk et al., 2013). Benchmark values are accurately reproduced for clear (Natraj and Hovenier, 2012) and cloudy atmospheres (Kokhanovsky et al., 2010) over a wavy reflecting surface and a black ocean (Emde et al., 2015). For pure Rayleigh atmospheres as in ocean-surface-atmosphere systems comparisons, the agreement is better than 1E-5 in intensity and 0.1% in

200 degree of polarization (Ramon et al., 2019; Chowdhary et al., 2020). The SMART-G code is capable of handling horizontal inhomogeneities of the albedo like adjacency effects (Chowdhary et al., 2019), or three-dimensional variations of the oceanic and atmospheric optical properties.

2.2.5 Differences in the Monte Carlo Methods

While all four models listed above use the Monte Carlo technique, there is one difference that can be noticed in the subsequent 205 comparisons. One option is to trace rays through the atmosphere, and calculate the scattering probability at each layer interface. This gives the possibility of photons not scattering and directly escaping the atmosphere, which is important for estimates of radiative fluxes (not directly applicable for limb scatter measurements). A consequence of this is that at higher wavelengths and higher tangent altitudes where the atmosphere is optically thin, a large number of photons are required to reduce the statistical noise to acceptable levels. In this study this technique is used by MYSTIC and SMART-G.

210 An alternative technique is to force every photon traced backwards from the observer to scatter. Random numbers are generated to determine the scatter location, not if scattering actually occurs. Photons can then be weighted by the optical thickness to account for the probability of scattering. A benefit of this technique is that the number of photons required to hit a desired noise floor is more uniform in wavelength and altitude space, but the technique is more specific to limb scattering measurements. Siro and SASKTRAN-MC both use the same force-scatter technique.

215 SMART-G includes an option to force additional scattering in limb mode, but only for the first (single) scatter. The option has a similar effect to the technique used by Siro/SASKTRAN-MC in that it reduces the variance of the calculation for optically thin scenarios, but it is not exactly equivalent.

Overall, all of the mentioned techniques solve the radiative transfer equation with the same level of accuracy. The only difference is the number of photons required to reach a desired level of precision. A more in-depth discussion of the computational 220 efficiency of the different techniques for different scenarios is presented in Sec. 4.5.

3 Model Test Cases

Test cases are designed to explore the aspects of the RTMs that are applicable for past, present, and future satellite-based limb-scattering measurements. All tests are performed for the following range of tangent altitudes, solar angles, surface reflectance, atmospheric constituent conditions, and wavelengths:

225 – 80 tangent altitudes from $0.5\,\mathrm{km}$ to $79.5\,\mathrm{km}$ (inclusive) with a spacing of $1\,\mathrm{km}$.

– 9 combinations of SZA and SAA which are given in Table 1.

– 3 values of a Lambertian Effective Reflectance of 0, 0.3, and 1.

– 3 atmospheric constituent conditions: pure Rayleigh scattering, Rayleigh scattering and ozone absorption, and Rayleigh + stratospheric aerosol scattering and ozone absorption

230 – 11 wavelengths provided in Table 2.

These test cases span the reasonable conditions that have been, or are currently, in use by operational limb scatter instruments for retrievals of typical atmospheric constituents.

In addition to different atmospheric and geometry conditions, test cases are selected using different RTM settings:

  – Single scattering, vector, no refraction

235 – Multiple scattering, scalar, no refraction

  – Multiple scattering, vector, refraction

Note that a single scattering scalar test case would be redundant as polarization only affects I through multiple scattering when the incident source is unpolarized. In all cases the SZA and SAA are defined at the tangent point of each individual line of sight. The placement of the tangent point assumes straight-line, un-refracted rays, from the observer.

240 One of the challenges in performing an inter-comparison of RTMs is ensuring that the inputs are the same across every model. In this study, care was taken so that the input parameters were specified in a way that can be assimilated by every model in the study. Stratospheric aerosol is specified as a log-normal distribution of Mie scattering particles with a median radius of 80 nm and a mode width of 1.6, with scattering parameters (cross sections, Mueller matrices, and Legendre moments) calculated using the code of Wiscombe (1980) and tabulated in wavelength. The refractive index is consistent with that of

245 sulfuric acid and is taken from Palmer and Williams (1975). Ozone absorption cross section is taken from measurements by Brion et al. (1993); Daumont et al. (1992); Malicet et al. (1995) interpolated to 243 K. Rayleigh scattering is assumed to be simple Rayleigh scattering without anisotropy corrections. These parameters are provided for reference in Table 2.

The background atmosphere is specified on a 1 km grid from 0 km to 100 km. The ozone profile is taken from a climatology derived from measurements from the Microwave Limb Sounder (Waters et al., 2006) and the Atmospheric Chemistry Exper-

250 iment (Bernath et al., 2005). Rayleigh scattering number density, pressure, and temperature are taken from typical tropical conditions in the MSIS-E-90 atmospheric model. The GLobal Space-based Stratospheric Aerosol Climatology (GLoSSAC, Thomason et al., 2018) is used to obtain a typical background aerosol extinction.

As noted in previous polarized RTM intercomparisons (e.g. Emde et al., 2015), the Stokes vectors returned by each RTM are not directly comparable due to differing conventions. A full discussion of differing conventions for reporting the Stokes

255 vector is beyond the scope of this study, and we refer to documentation on each model for specifics on how each individual RTM defines the Stokes vector. For consistency in this study all Stokes parameters are converted to follow the definition of Hovenier et al. (2004), which for the models included differs only by the sign of Q, U, and/or V. The signs applied to the Stokes parameters from each of the models are shown in Table 3.

3.1 A Note on Atmospheric Gridding

260 The test cases specify the atmospheric state parameters on a 1 km grid from 0 km to 100 km, but leave the interpolation scheme up to the individual RTM. The two standard choices either assume that the atmospheric state varies linearly between grid points,

Table 1. Solar zenith angles, solar azimuth angles, and solar scattering angles used in the test cases.

SZA	SAA	SSA
10°	20°	80.6°
15°	70°	84.9°
35°	90°	90.0°
45°	50°	63.0°
50°	130°	119.5°
60°	70°	72.8°
70°	30°	35.5°
80°	60°	60.5°
80°	150°	148.5°

Table 2. The Rayleigh scattering cross-section, ozone absorption cross-section, and stratospheric aerosol refractive index used for the test cases.

Wavelength [nm]	Rayleigh Cross-Section [cm^2]	Ozone Cross-Section [cm^2]	Aerosol Refractive Index
300	5.602831e-26	3.626519e-19	1.452272 - 0i
315	4.549917e-26	4.218142e-20	1.449746 - 0i
351	2.878846e-26	1.225798e-22	1.449180 - 1.33565e-05i
435	1.177405e-26	8.362497e-23	1.434603 - 4.90115e-05i
442	1.102286e-26	1.698570e-22	1.433675 - 5.10270e-05i
525	5.438003e-27	2.183215e-21	1.429252 - 6.51460e-05i
600	3.156146e-27	5.206045e-21	1.429088 - 6.46200e-05i
675	1.957387e-27	1.505802e-21	1.428480 - 5.44275e-05i
943	5.069933e-28	0	1.423274 - 0i
1020	3.692419e-28	0	1.421113 - 0i
1700	4.611621e-29	0	1.396316 - 4.33650e-04i

or that the atmosphere consists of $1\,\mathrm{km}$ homogeneous layers where the atmospheric state parameters are constant. How the discretized atmospheric state maps to an effective continuous quantity is of particular importance since any retrieved quantity must be interpreted the same way.

265   The RTMs GSLS, SASKTRAN (HR and MC), and Siro assume linear interpolation and handle it through analytic methods. All four models calculate optical depth exactly, assuming a linearly varying extinction (see Oikarinen et al., 1999; Loughman et al., 2015, for more detail). For SASKTRAN-MC and Siro this is all that is required and the linear variation of the atmosphere is accounted for without approximation. GSLS and SASKTRAN-HR must make additional approximations in the calculation

Atmospheric
Measurement
Techniques
Discussions
Open Access
EGU

Table 3. Sign that each models Stokes parameters were multiplied by to follow the definition of Hovenier et al. (2004). A "-" indicates that the component was multiplied by -1, while a "+" indicates the component was unchanged.

Model	Q	U
GSLS	-	+
MYSTIC	+	-
SASKTRAN (MC/HR)	-	+
SCIATRAN	+	+
Siro	-	+
SMART-G	+	-

of the source function and we refer back to Loughman et al. (2015) and Zawada et al. (2015) respectively for the exact methods
270 used.

The other RTMs (MYSTIC, SCIATRAN, SMART-G) use homogeneous layers. To compare the models more directly, the RTMs using homogeneous layers have been configured using sub-layers with linear interpolation. Figure 2 shows an example of how using $1000\,\mathrm{m}$ or $250\,\mathrm{m}$ homogeneous shells vary compared to $100\,\mathrm{m}$ shells within MYSTIC. Layering using $1000\,\mathrm{m}$ shells introduces errors on the order of $0.5\,\%$ at $351\,\mathrm{nm}$ in regions where the atmosphere is optically thin, while the error
275 using $250\,\mathrm{m}$ shells is $0.1\,\%$. For all future calculations both MYSTIC and SMART-G have been configured to use $250\,\mathrm{m}$ shells. SCIATRAN uses a hybrid system where sub-gridding is applied only to the first three layers near the beginning of each integration line and three layers above the tangent point (the exact number of layers is an input parameter).
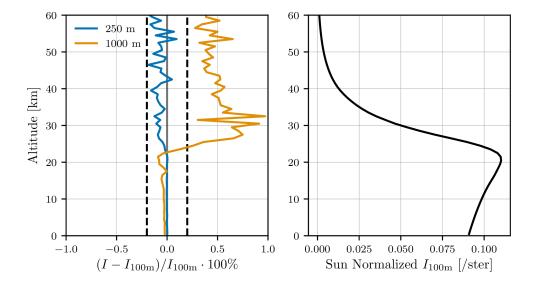
4   Discussion and Results

The main challenge in interpreting, and attributing, differences between models is that the true answer is not known. All
280 comparisons shown in this section are relative to what we have called the Multi-Model Mean (MMM). The MMM is composed of the set of models that agree with each other to a level that cannot be attributed to a concrete difference in a single model. For the single scattering test cases the level was determined to be $0.2\,\%$, and $1\,\%$ for the multiple scattering test cases. Any RTM that is found to have disagreements above these levels is excluded from the MMM for the relevant test case, causing the models composing the MMM to vary between different test cases.
285 While tests were performed for both vectorial and scalar modes, no significant differences were found in agreement between the models in scalar or vector mode. Therefore, for the purpose of brevity, no comparisons of strictly scalar mode are shown. It is understood that the results for the polarised comparisons are equally applicable to scalar calculations.

Figure 2. (Left Panel) Percent difference in single scattered radiance when MYSTIC is using $1000\,\mathrm{m}$ or $250\,\mathrm{m}$ homogeneous shells compared to $100\,\mathrm{m}$ homogeneous shells. (Right Panel) The sun-normalized radiance computed using $100\,\mathrm{m}$ shells. The atmosphere contains Rayleigh scattering, ozone absorption, and stratospheric aerosol Mie scattering with a SZA of $70°$ and a SAA of $30°$. Refraction is disabled. MYSTIC was configured to use 100 million photons. Dashed vertical lines indicate $\pm 0.2\,\%$ levels.

4.1 Single Scatter

Simplifying assumptions made for the single scatter calculation are minimal, and thus we expect differences to be relatively
290 small. We do not expect zero differences due to the various methods of gridding in the vertical dimension of the atmosphere.
As originally done in the limb geometry by Siro (Oikarinen et al., 1999) and discussed extensively in Loughman et al. (2004,
2015), the calculation of optical depth may be performed analytically assuming an extinction that varies linearly in altitude.
However, the integration of the source function cannot be performed the same way and an approximation must be made. For
example, SASKTRAN-HR creates a second order spline of the source function across an integration cell (Zawada et al., 2015),
295 but other models may assume a constant source function or do something more sophisticated. All of this is further complicated
by any form of sub-gridding the model may perform in order to obtain a more accurate result.

Differences for the most extreme single scatter case (Rayleigh + ozone + stratospheric aerosol) are shown in Fig. 3. Differences are presented relative to the mean of the three deterministic models (SASKTRAN-HR, GSLS, and SCIATRAN), which
we refer to as the Multi-Model Mean (MMM). We chose to use the deterministic models as the reference because statistical
300 errors in the single scatter case are on the order of the differences observed between the different models. For all conditions,
errors between the three deterministic models are less than $0.1\,\%$. The differences between GSLS, SASKTRAN-HR, and SCI-
ATRAN are likely due to the slightly different gridding techniques. For the statistical models MYSTIC, SASKTRAN-MC,
SMART-G, and Siro no errors are detected that are greater than the random noise present ($\sim 0.2\,\%$ in most cases). One thing

to note about the SMART-G calculation is that statistical errors are correlated in solar geometry, while for the other MC mod-
els the errors are uncorrelated. Errors are correlated because the SMART-G calculation considered multiple solar positions
simultaneously in a single calculation, while the other models performed each line of sight and solar position independently.

The excellent agreement in single scatter is expected due to the relative simplicity of the calculation. Fundamentally each
RTM solves the single scatter problem in the same way with minimal assumptions, the primary purpose of this test is to ensure
that the inputs to RTM are configured correctly. The agreement of 0.1–0.2 % here sets a baseline that differences above this
level in more complex test cases cannot be explained by differing treatment of input data.

4.2 Multiple Scatter

Differences in multiple scatter are expected to be larger than those seen in single scatter owing to the extra complexity of the
radiative transfer problem. The discrete models must deal with discretizations of the multiple scattering source term and may
also make fundamental approximations for the sake of computational speed. Comparatively the statistical models employ a
simpler technique.

In Fig. 4 we see that differences between each RTM and the MMM (MYSTIC, SASKTRAN-HR, SASKTRAN-MC, SCI-
ATRAN, and SMART-G) is usually less than 1 % with a few exceptions. Siro shows a low bias on the order of 1–4 % at 351
nm, which is most pronounced at low solar zenith angles. The bias is not present when the Lambertian surface albedo is set
to 0 instead of 1. This bias was present in Loughman et al. (2004), however it was misattributed to a high bias in the other
RTMs as Siro was used as the reference model. Internal testing suggests that the difference may not be directly related to
ground scattering, and instead is an error that compounds on each succesively higher order of scatter. The error is strongest
near 351 nm and a surface albedo of 1 because this is the condition where higher orders of scatter have the largest contribution
to the observed radiance.

GSLS at 351 nm has a distinct pattern in altitude with variations on the order of 1 % that are relatively consistent across
solar geometry. The exact cause of these variations are unknown but are likely caused by discretizations of the multiple scatter
source field calculation, however as stated these variations are fairly small. At 675 nm GSLS shows significant deviations of
up to 4 % depending on the solar geometry at altitudes near 25 km. The deviation is only present when the Lambertian surface
albedo is 1 and is almost non-existent with a 0 albedo. Testing has shown that the difference is present for all atmospheric
composition scenarios and is thought to be due to approximations made in the ground to line of sight scatter calculation.

SASKTRAN (HR and MC), SCIATRAN, SMART-G, and MYSTIC all agree for all conditions to better than 1 %. As stated,
differences less than 1 % are difficult to attribute to any particular RTM due to both not having a precise reference model
and the inherent statistical noise. However, we do note that SASKTRAN-HR and SCIATRAN both have altitude variation
patterns on the order of 0.5 % that are constant across solar geometry but differ in wavelength. MYSTIC, SASKTRAN-MC,
and SMART-G are indistinguishable at the level of statistical noise. The general agreement between the models is better than
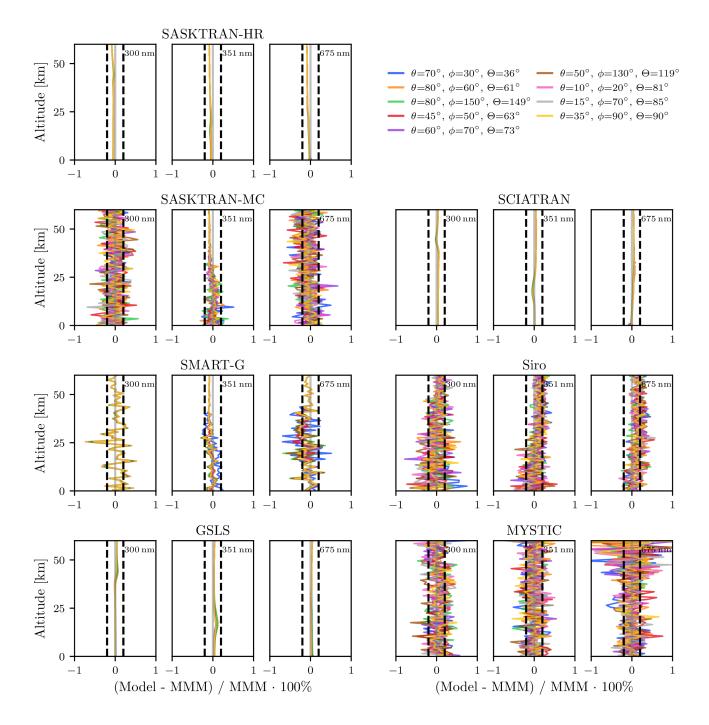has been observed before in comparisons of RTMs in limb scatter geometry even for scalar cases.

Figure 3. Percent differences in single scatter I relative to the MMM (GSLS, SASKTRAN-HR, and SCIATRAN) for each RTM at a variety of wavelengths and solar conditions. The atmospheric optical properties include Rayleigh scattering, ozone absorption, and stratospheric aerosol Mie scattering. Refraction is disabled. Dashed vertical lines indicate $\pm 0.2\,\%$
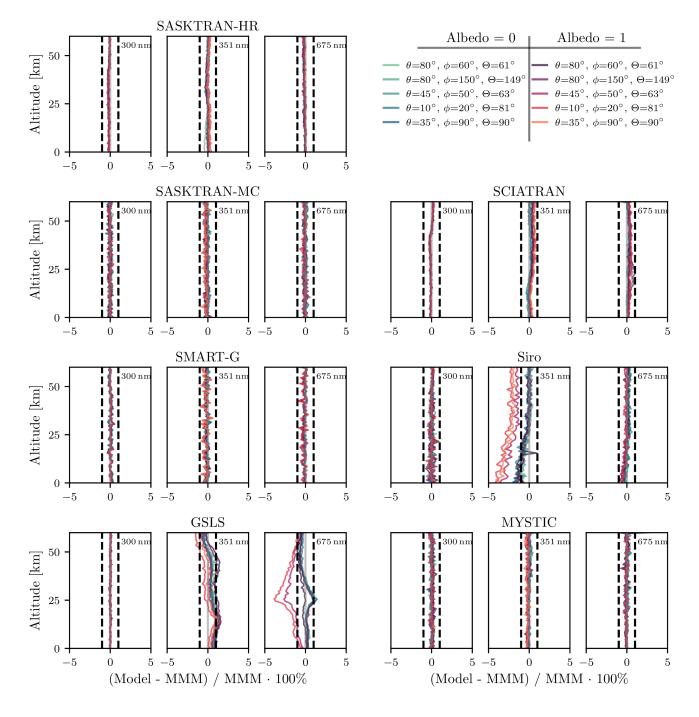
Atmospheric
Measurement
Techniques
Open Access

EGU

Discussions

Figure 4. Percent differences in I relative to the MMM (MYSTIC, SASKTRAN-HR, SASKTRAN-MC, SCIATRAN, and SMART-G) for each RTM at a variety of wavelengths and solar conditions. The atmospheric optical properties include Rayleigh scattering, ozone absorption, and stratospheric aerosol Mie scattering. Refraction is disabled. Dashed vertical lines indicate $\pm 1\%$ levels.

Atmospheric
Measurement
Techniques

Open Access

EGU

Discussions

4.3 Stokes Parameters

While all comparisons so far have involved vector radiative transfer calculations only differences in the I component of the Stokes vector have been analyzed. Agreement in I is indicative that the polarization implementation in each model is sensible, however polarization can be investigated more rigorously by analyzing the individual Stokes parameters. Figure 5 shows the individual Stokes components, and their differences to the MMM (MYSTIC, SMART-G, and SASKTRAN-MC), for one scenario with large polarization (scattering angle near $90\,°$, albedo 0) and one scenario with low polarization (scattering angle away from $90\,°$, albedo 1).

Generally agreement between Q, U, and the linear polarization, $\sqrt{Q^2 + U^2}$, is worse than the agreement with I. MYSTIC, SASKTRAN-MC, and SMART-G agree for all components at the level of statistical noise ($\sim$0.2–1%), while Siro shows deviations at altitudes below $30\,\mathrm{km}$ that can approach $5\,\%$ depending on the condition. SASKTRAN-HR and SCIATRAN are usually within $1\,\%$ for the cases shown, however in some situations this can exceed $1\,\%$. In cases where the polarization is small, GSLS can show deviations of 2–4 %, but these disappear in the cases with high linear polarization. The differences observed in linear polarization sometimes mirror differences observed in I, and are sometimes independent.

In order to isolate the polarization effects, we consider two quantities: the Degree of Linear Polarization (DOLP) and the Linear Polarization Orientation (LPO). DOLP is defined as

$$\mathrm{DOLP} = \frac{\sqrt{Q^2 + U^2}}{I}, \tag{1}$$

which is the fraction of radiation that is linearly polarized, and LPO is defined as

$$\mathrm{LPO} = \frac{1}{2}\arctan\frac{U}{Q}, \tag{2}$$

which indicates the direction of linear polarization. The absolute differences in DOLP and LPO for the Rayleigh scattering, ozone absorption, and stratospheric aerosol scattering case are shown in Fig. 6 and Fig. 7 respectively.

Differences in the DOLP and LPO are overall small, with a few exceptions. Once again, the MC models MYSTIC, SASKTRAN-MC, and SMART-G agree in all cases to the level of statistical noise in the computation. At $300\,\mathrm{nm}$ no differences are observed between the models as the majority of the signal is single scatter. GSLS, SASKTRAN-HR, and SCIATRAN all have minor spreads in DOLP at $351\,\mathrm{nm}$ depending on solar angle and albedo on the order of 0.002. SCIATRAN shows differences in LPO at $351\,\mathrm{nm}$ of $0.2\,°$ for some conditions, however these are conditions where the overall polarization signal is small. At $675\,\mathrm{nm}$ GSLS has differences in DOLP of up to 0.02 when the surface albedo is 1, which are likely related to the differences in I observed previously. For the same wavelength the LPO shows deviations on the order of $0.5\,°$ for the high surface albedo case.

Siro has differences in DOLP, but curiously does not have any significant differences in LPO. At $351\,\mathrm{nm}$, deviations in DOLP are up to 0.03 and are present at all albedos and solar conditions, but are larger at high albedo and low solar zenith angle. The deviations are largest at conditions where there was significant differences in I, but do not share the same shape. There are differences of up to 0.02 at $675\,\mathrm{nm}$ in DOLP between Siro and the MMM, however the differences are only present at low albedos. The differences are largely eliminated when aerosol is removed from the atmosphere (not shown) suggesting that it could be due to aerosol multiple scattering.
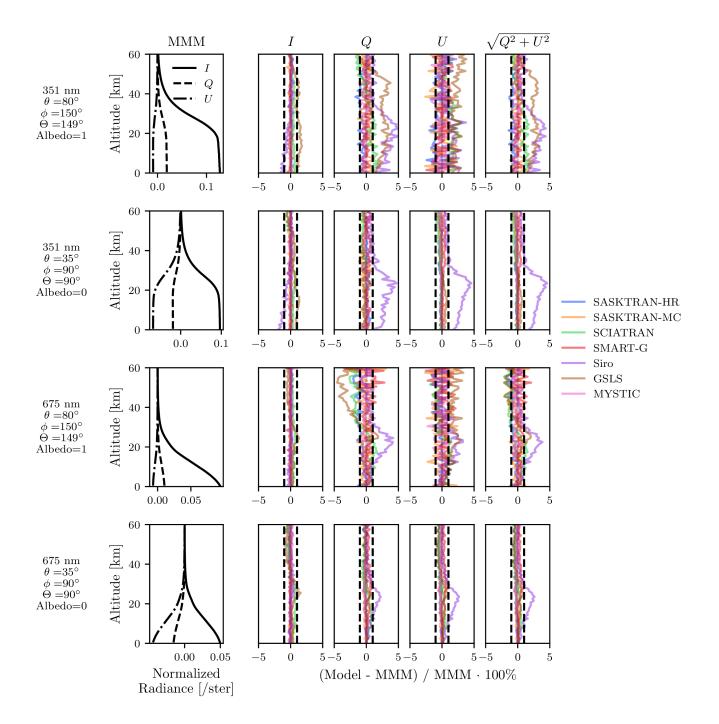
Figure 5. Left most column: The MMM calculation of I, Q, and U for four different scenarios consisting of MYSTIC, SASKTRAN-MC, and SMART-G. Other columns: percent difference in I, Q, U, and $\sqrt{Q^2 + U^2}$ for each model relative to the MMM. The atmospheric optical properties include Rayleigh scattering, ozone absorption, and aerosol scattering. Dashed vertical lines indicate $\pm 1\%$ levels.

Atmospheric
Measurement
Techniques
Discussions
EGU
Open Access

Both SASKTRAN (HR and MC) and GSLS make the assumption that V is identically 0, which reduces the size of the phase
370 matrix to speed up the computation, and it does not appear that this approximation affects the results in a noticeable way. The
comparison atmospheres only include smaller spherical scatterers (Mie and Rayleigh scattering), and do not include larger
particles as would be seen in ice clouds for example. It is possible that the approximation of neglecting V would break down
under conditions containing larger particles, droplets or crystals.

4.4 Refraction

375 All of the models considered thus far with the exceptions of SASKTRAN-MC and MYSTIC support atmospheric refraction
to some level. While Siro has support for refraction it was not tested as part of this study. GSLS and SASKTRAN-HR neglect
refraction of the incoming solar rays. Furthermore GSLS and SASKTRAN-HR neglect refraction for multiple scattering effects,
only implementing refraction for the line of sight ray. SCIATRAN and SMART-G implement refraction in a generic way
accounting for all solar and multiple scattering effects. SASKTRAN-HR has since been updated to include refractive effects
380 for incoming solar rays and multiple scatter effects but the calculations here use only line of sight refraction.

Differences in the multiple scatter signal when refraction is enabled for the stratospheric aerosol scattering case are shown
in Fig. 8. At 351 nm the effect of refraction is minimal and agreement is identical to the cases without refraction; however, at
longer wavelengths several differences are observed between the RTMs. SMART-G has a discontinuity in the signal at 11.5 km
causing differences on the order of 1 % relative to SASKTRAN-HR and SCIATRAN. GSLS shows similar differences in the
385 refracted and unrefracted cases, indicating that the refractive effect is similar to that of SASKTRAN-HR and SCIATRAN.

To further investigate these differences, the ratio of refracted to unrefracted I for a single condition for each model is
shown in Fig. 9. This refraction ratio was found to be insensitive to the solar geometry, albedo, and atmospheric composition.
The refraction ratio is larger at longer wavelengths due to the atmosphere being more optically thin, however the 1020 nm
wavelength as shown in the figure is representative of the differences observed between the models at all wavelengths. GSLS,
390 SASKTRAN-HR, and SCIATRAN show excellent agreement in the refraction ratio, with differences being insignificant next
to the already observed differences between the models. The refractive enhancement in SMART-G is 1–2 % less than GSLS,
SASKTRAN-HR, and SCIATRAN with the exception of a discontinuity near 11.5 km that greatly enhances the refractive
enhancement for a few km below. Possible reasons for the differences of SMART-G compared to GSLS, SASKTRAN-HR,
and SCIATRAN are still under investigation.

395 There are several possible reasons for the small observed differences between GSLS, SASKTRAN-HR and SCIATRAN.
The index of refraction of the atmosphere was not harmonized between the models, instead each model performed internal
calculations using the provided atmospheric temperature and pressure. There exist various methods to do this calculation
and they may not be the same between each RTM. Differing methods of ray-tracing and integration can also lead to small
differences. Since SCIATRAN (and SMART-G) included refractive effects for the incoming solar ray and multiple scatter
400 terms, it is possible that this could be the source of some minor differences. The solar geometries tested here have been limited
to SZA $\leq 80°$, where refraction of the incoming solar ray is expected to be minimal. Further study could examine the effect
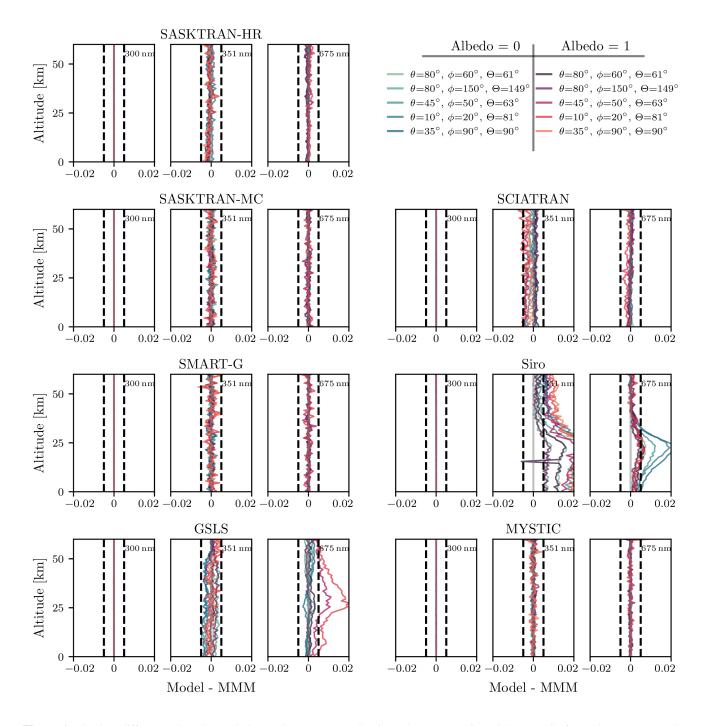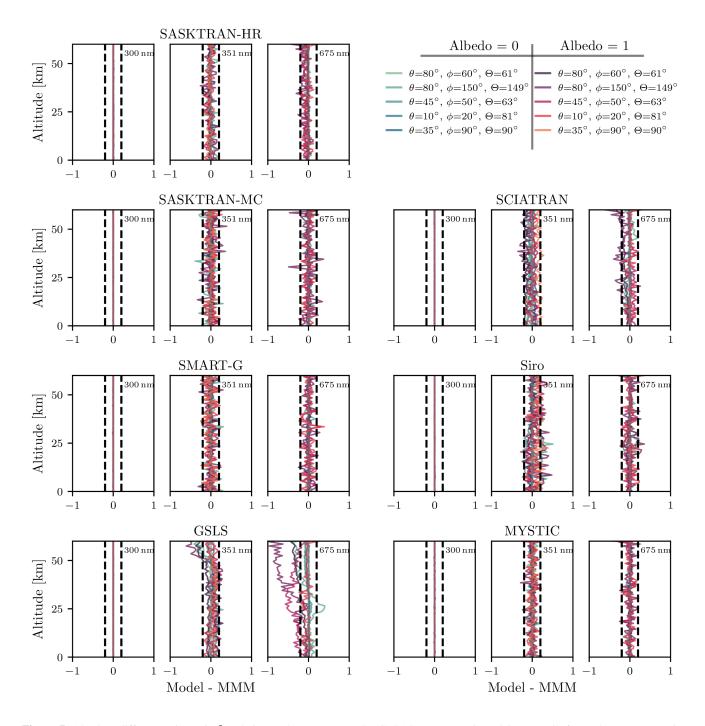of refraction at higher solar zenith angles.

Figure 6. Absolute differences in DOLP relative to the MMM (MYSTIC, SASKTRAN-MC, and SMART-G) for each RTM at a variety of wavelengths and solar conditions. The atmospheric optical properties include Rayleigh scattering, ozone absorption, and stratospheric aerosol Mie scattering. Refraction is disabled. Dashed vertical lines indicate ±0.005 levels.

Figure 7. Absolute differences in LPO [°] relative to the MMM (MYSTIC, SASKTRAN-MC, and SMART-G) for each RTM at a variety of wavelengths and solar conditions. The atmospheric optical properties include Rayleigh scattering, ozone absorption, and stratospheric aerosol Mie scattering. Refraction is disabled. Dashed vertical lines indicate $\pm 0.2°$ levels.
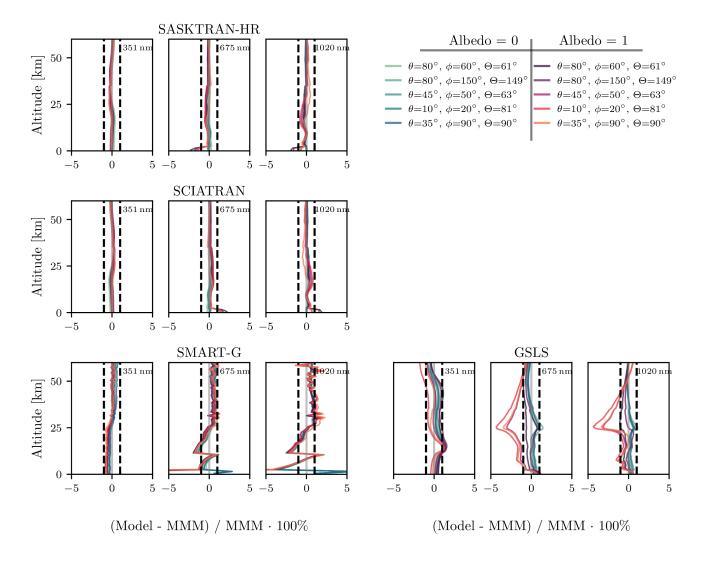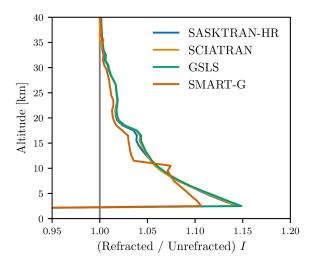
Figure 8. Same as Fig. 4 but with refraction enabled. The MMM is composed of SASKTRAN and SCIATRAN. Dashed vertical lines indicate ±1% levels.

Figure 9. Ratio of refracted to unrefracted I for multiple scatter, Rayleigh scattering + ozone absorption + stratospheric aerosol scattering, SZA=70°, SAA=30°, and a Lambertian surface reflectance of 0 at 1020 nm for every model that supports refraction.

4.5 Timing

We have considered a basic run time comparison between the models in the study. While a useful exercise, there are technical challenges in standardizing the hardware used to execute the models, and in the case of SMART-G which uses a GPU the standardization is not possible. More importantly every model has settings that involve an accuracy/speed trade-off. For example, with the deterministic models, there are various discretization setting that can dramatically affect the speed of the calculations.

Harmonizing the balance between accuracy and speed between all of the RTMs is impractical, instead we opt for a simple order of magnitude timing estimate. The time taken to execute all of the multiple scatter polarized tests for each model without refraction is shown in Table 4. These timing numbers should be interpreted as the time required to execute a wide variety of test cases, individual RTMs may be significantly more or less efficient in specific cases, however analyzing these differences is beyond the scope of this study. For the CPU based models a scaled runtime value is also supplied where the runtime on equivalent hardware has been approximated using the relative CPU benchmark values from https://www.passmark.com/. The deterministic models, GSLS, SCIATRAN, and SASKTRAN-HR, all have runtimes of a similar order of magnitude taking anywhere from 0.3 s to 1 s to execute a single wavelength, solar geometry, and atmospheric composition on average.

Analyzing the timing of the Monte Carlo models is inherently more challenging as the calculations also contain statistical noise. It is common to benchmark models for a set number of photons, however the number of photons used is not comparable between Siro/SASKTRAN-MC and MYSTIC/SMART-G since the MC technique is not the same. Instead, the precision of the calculation must be directly compared, which is shown for a typical condition in Fig. 10. For the precision estimation and timing, MYSTIC was configured to use a constant 1E6 photons. The other models (SASKTRAN-MC, Siro, and SMART-G)

Table 4. Estimated time to execute all multiple scatter no refraction tests. This includes three effective surface albedos, three different atmospheric compositions, 11 wavelengths, 9 solar geometries, and 80 lines of sight. The MC models were executed to the precision shown in Fig. 10 (see text for more detail). [a] The scaled runtime is calculated by scaling every CPU to the computational power of the AMD 3900x using the relative benchmark values from https://www.passmark.com/ as of November 6th 2020.

Model	Hardware Description	Time [minutes]	Scaled Runtime[a] [Minutes]
GSLS	Two Intel Xeon E5-2630 (6 physical cores at 2.3 GHz each)	35	13.0
SASKTRAN-HR	AMD 3900x (12 physical cores at 3.8 GHz)	7.4	7.4
SCIATRAN	Intel i7-6850 (6 physical cores at 3.6 GHz)	13.5	4.6
SASKTRAN-MC	AMD 3900x (12 physical cores at 3.8 GHz)	1909	1909
Siro	Four Intel Xeon E5-2630 (8 physical cores at 2.4 GHz each)	16560	20078
MYSTIC	AMD 3900x (12 physical cores at 3.8 GHz)	1906	1906
SMART-G	NVIDIA Titan V	59.2	N/A

were configured identically to the previous radiance comparisons. Siro used a constant 1E6 photons, while SASKTRAN-MC and SMART-G used a variable number of photons targeting 0.2–0.3% precision.

For the given precisions, The CPU based statistical models, MYSTIC, SASKTRAN-MC, and Siro, have runtimes within an order of magnitude. The runtime of Siro appears large, however the precision is generally better. Approximately scaling the

425 Siro calculation to 0.2% precision would result in a speed increase of a factor of ∼4. Because of the differences in precision between the different calculations we won't attempt to quantify small differences between the MC models. One thing of particular interest is the general efficiency between the technique used by Siro/SASKTRAN-MC and MYSTIC/SMART-G. Both Siro and MYSTIC used a constant 1E6 photons for all conditions, however the precision of Siro is relatively constant in altitude and wavelength hovering around 0.1%, while the precision of MYSTIC varies significantly. MYSTIC achieved better

430 than 0.1% precision in cases where the atmosphere heavily scatters (low altitudes, shorter wavelengths), and worse precision at higher altitudes and longer wavelengths where the atmosphere is optically thin. As mentioned earlier, this is since photons in Siro are forced to scatter, while photons in MYSTIC may pass through the atmosphere without interaction.

The runtime for the GPU based MC model, SMART-G, is ∼1–2 orders of magnitude less than the other MC models. The most natural comparison is between SMART-G and SASKTRAN-MC since they have similar precision for this case. Here,

435 SMART-G achieves a speedup of ∼30x relative to SASKTRAN-MC on the hardware used. SMART-G only forces scatter events to happen on the first order of scatter (contrary to SASKTRAN-MC and Siro which force scatters on all orders), but it appears that this is sufficient to obtain reasonable precision in all scenarios.
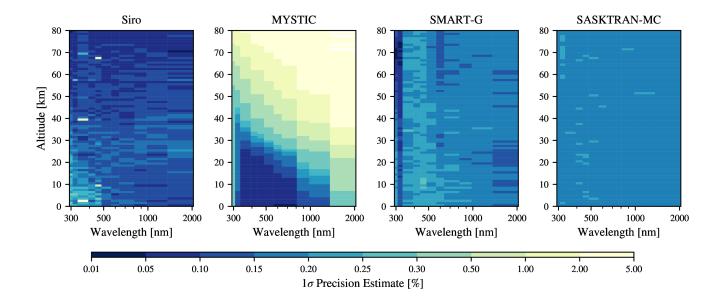
5 Conclusions

A systematic comparison has been performed between seven radiative transfer models operating in the limb scatter geometry.

440 The seven models are capable of handling the sphericity of the atmosphere, and compute the Stokes vector accounting for

Figure 10. Precision estimates for the MC models for multiple scatter, Rayleigh scattering + ozone absorption + stratospheric aerosol scattering, SZA=70°, SAA=30°, and a Lambertian surface reflectance of 1. Precision estimates for MYSTIC, SASKTRAN-MC, and SMART-G were taken from the model output. Siro precision was estimated by running the above scenario 20 times and taking the standard deviation.

polarisation. The test cases cover a wide variety of solar angles, Rayleigh scattering, ozone absorption, Mie scattering, and surface reflectances.

In single scatter, the deterministic models GSLS, SASKTRAN-HR, and SCIATRAN agree within 0.1 % for all observed conditions. The statistical models MYSTIC, SASKTRAN-MC, Siro, and SMART-G all agree to a level better than the precision of the calculation which is approximately ∼0.2 %.

For almost all conditions in multiple scatter, the agreement between the fully spherical models in the multiple scatter cases is within 1% when refraction is disabled for I with a few exceptions:

- Siro can have disagreement of up to 3 % at shorter wavelengths, particularly when the solar zenith angle is low and the surface reflectance is high. The difference manifests as a low bias in the radiance, and a high bias in the degree of linear polarization. The cause of this bias is currently unknown.

- At longer wavelengths in all atmospheric conditions and when the Lambertian surface reflectance is high, GSLS shows biases of up to 3 % that are dependent on solar geometry. The bias is thought to be caused by approximations made in the direct ground to line of sight scattering calculation.

Refraction has been tested for GSLS, SASKTRAN-HR, SMART-G, and SCIATRAN. The refractive effect among all models is almost indistinguishable, with the exception of a ∼1 % discontinunity in radiance in the SMART-G calculation at 11.5 km when refraction is enabled. The cause of the discontinuity is currently unknown.

Differences in quantities representing linear polarization, the DOLP and LPO, have also been assessed, however the results are more difficult to interpret. The MC models MYSTIC, SASKTRAN-MC, and SMART-G agree within statistical noise for all considered conditions and serve as a combined reference. SASKTRAN-HR and SCIATRAN generally agree with the reference at a level of 0.002 in DOLP and $0.2\,°$ in LPO, with the largest deviations in LPO being in conditions where the linearly polarized signal is small. For most conditions, GSLS agrees at a similar level, with the exception of high Lambertian surface albedos at longer wavelengths where DOLP can vary up to 0.02, and LPO by $0.5\,°$. Siro shows deviations in DOLP at both $351\,\mathrm{nm}$ and $675\,\mathrm{nm}$ that approach 0.03, but has no distinguishable difference from the reference in LPO.

Overall the agreement between the models is excellent, and is better than has been reported for scalar comparisons in the past. The agreement provides additional confidence in the retrievals from limb scatter instruments such as OMPS-LP, OSIRIS, and SCIAMACHY. In particular, confidence in modelling the polarized signal is important for the upcoming ALTIUS mission which is linearly polarized.

There are several areas where future studies comparing RTMs in the limb viewing geometry could expand upon. Scattering from larger, non-spherical, particles, droplets, or crystals should be assessed which may result in larger differences in particular for circular polarization. More extreme cases with larger solar zenith angles may be checked, in particular to determine the effect of refraction at higher solar zenith angles.

Data availability. The input atmospheric data, test cases, and the results for each model are made publicly available as Zawada et al. (2020).

Author contributions. D.Z. wrote the initial draft of the manuscript. Model runs were performed by D.Z., G.F., R.L., A.M., and A.R.. All authors contributed in designing the study, interpreting the results, and revising the manuscript.

Competing interests. No competing interests are present.

Atmospheric
Measurement
Techniques
Discussions

References

Arosio, C., Rozanov, A., Malinina, E., Eichmann, K.-U., von Clarmann, T., and Burrows, J. P.: Retrieval of ozone profiles from OMPS
limb scattering observations, Atmospheric Measurement Techniques, 11, 2135–2149, https://doi.org/10.5194/amt-11-2135-2018, https:
//www.atmos-meas-tech.net/11/2135/2018/, 2018.

Bernath, P. F., McElroy, C. T., Abrams, M. C., Boone, C. D., Butler, M., Camy-Peyret, C., Carleer, M., Clerbaux, C., Coheur, P. F., Colin,
R., DeCola, P., DeMazière, M., Drummond, J. R., Dufour, D., Evans, W. F., Fast, H., Fussen, D., Gilbert, K., Jennings, D. E., Llewellyn,
E. J., Lowe, R. P., Mahieu, E., McConnell, J. C., McHugh, M., McLeod, S. D., Michaud, R., Midwinter, C., Nassar, R., Nichitiu, F.,
Nowlan, C., Rinsland, C. P., Rochon, Y. J., Rowlands, N., Semeniuk, K., Simon, P., Skelton, R., Sloan, J. J., Soucy, M. A., Strong, K.,
Tremblay, P., Turnbull, D., Walker, K. A., Walkty, I., Wardle, D. A., Wehrle, V., Zander, R., and Zou, J.: Atmospheric chemistry experiment
(ACE): Mission overview, Geophysical Research Letters, 32, L15S01, https://doi.org/10.1029/2005GL022386, http://doi.wiley.com/10.
1029/2005GL022386, publisher: Wiley-Blackwell ISBN: 0094-8276, 2005.

Bourassa, A. E., Degenstein, D. A., Gattinger, R. L., and Llewellyn, E. J.: Stratospheric aerosol retrieval with opti-
cal spectrograph and infrared imaging system limb scatter measurements, Journal of Geophysical Research, 112, D10217,
https://doi.org/10.1029/2006JD008079, 2007.

Bourassa, A. E., Degenstein, D. A., and Llewellyn, E. J.: SASKTRAN: A spherical geometry radiative transfer code for
efficient estimation of limb scattered sunlight, Journal of Quantitative Spectroscopy and Radiative Transfer, 109, 52–73,
https://doi.org/10.1016/j.jqsrt.2007.07.007, 2008.

Bovensmann, H.: SCIAMACHY: Mission objectives and measurement modes, Journal of the atmospheric sciences, pp. 127–150, 1999.

Brion, J., Chakir, A., Daumont, D., Malicet, J., and Parisse, C.: High-resolution laboratory absorption cross section of O3. Temperature
effect, Chemical physics letters, 213, 610–612, publisher: Elsevier, 1993.

Buras, R. and Mayer, B.: Efficient unbiased variance reduction techniques for Monte Carlo simulations of radiative trans-
fer in cloudy atmospheres: The solution, Journal of Quantitative Spectroscopy and Radiative Transfer, 112, 434–447,
https://doi.org/10.1016/j.jqsrt.2010.10.005, http://www.sciencedirect.com/science/article/pii/S0022407310003791, 2011.

Butz, A., Bösch, H., Camy-Peyret, C., Chipperfield, M., Dorf, M., Dufour, G., Grunow, K., Jeseck, P., Kühl, S., Payan, S., Pepin, I., Pukite, J.,
Rozanov, A., von Savigny, C., Sioris, C., Wagner, T., Weidner, F., and Pfeilsticker, K.: Inter-comparison of stratospheric O_3 and NO_2 abun-
dances retrieved from balloon borne direct sun observations and Envisat/SCIAMACHY limb measurements, Atmospheric Chemistry and
Physics, 6, 1293–1314, https://doi.org/https://doi.org/10.5194/acp-6-1293-2006, https://acp.copernicus.org/articles/6/1293/2006/, pub-
lisher: Copernicus GmbH, 2006.

Chowdhary, J., Zhai, P.-W., Boss, E., Dierssen, H., Frouin, R., Ibrahim, A., Lee, Z., Remer, L. A., Twardowski, M., Xu, F., Zhang, X., Otta-
viani, M., Espinosa, W. R., and Ramon, D.: Modeling Atmosphere-Ocean Radiative Transfer: A PACE Mission Perspective, Frontiers in
Earth Science, 7, https://doi.org/10.3389/feart.2019.00100, https://www.frontiersin.org/articles/10.3389/feart.2019.00100/full, publisher:
Frontiers, 2019.

Chowdhary, J., Zhai, P.-W., Xu, F., Frouin, R., and Ramon, D.: Testbed results for scalar and vector radiative transfer com-
putations of light in atmosphere-ocean systems, Journal of Quantitative Spectroscopy and Radiative Transfer, 242, 106717,
https://doi.org/10.1016/j.jqsrt.2019.106717, http://www.sciencedirect.com/science/article/pii/S002240731930370X, 2020.

Cisewski, M., Zawodny, J., Gasbarre, J., Eckman, R., Topiwala, N., Rodriguez-Alvarez, O., Cheek, D., and Hall, S.: The Stratospheric
Aerosol and Gas Experiment (SAGE III) on the International Space Station (ISS) Mission, in: Sensors, Systems, and Next-Generation

520   Satellites XVIII, vol. 9241, p. 924107, International Society for Optics and Photonics, https://doi.org/10.1117/12.2073131, https://www.
       spiedigitallibrary.org/conference-proceedings-of-spie/9241/924107/The-Stratospheric-Aerosol-and-Gas-Experiment-SAGE-III-on-the/
       10.1117/12.2073131.short, 2014.

Daumont, D., Brion, J., Charbonnier, J., and Malicet, J.: Ozone UV spectroscopy I: Absorption cross-sections at room temperature, Journal
       of Atmospheric Chemistry, 15, 145–155, publisher: Springer, 1992.

525   Degenstein, D. A., Bourassa, A. E., Roth, C. Z., and Llewellyn, E. J.: Limb scatter ozone retrieval from 10 to 60 km using a multiplicative
       algebraic reconstruction technique, Atmospheric Chemistry and Physics, 9, 6521–6529, https://doi.org/10.5194/acp-9-6521-2009, 2009.

Dueck, S. R., Bourassa, A. E., and Degenstein, D. A.: An efficient algorithm for polarization in the SASKTRAN radiative trans-
       fer framework, Journal of Quantitative Spectroscopy and Radiative Transfer, 199, 1–11, https://doi.org/10.1016/j.jqsrt.2017.05.016,
       https://www.sciencedirect.com/science/article/pii/S0022407317301863, publisher: Pergamon, 2017.

530   Elash, B., Bourassa, A., Rieger, L., Dueck, S., Zawada, D., and Degenstein, D.: The sensitivity to polarization in stratospheric aerosol
       retrievals from limb scattered sunlight measurements, Journal of Quantitative Spectroscopy and Radiative Transfer, 189, 75–85,
       https://doi.org/10.1016/j.jqsrt.2016.11.014, http://linkinghub.elsevier.com/retrieve/pii/S0022407316304976, 2017.

Elash, B. J., Bourassa, A. E., Loewen, P. R., Lloyd, N. D., and Degenstein, D. A.: The Aerosol Limb Imager: acousto-optic imaging of
       limb-scattered sunlight for stratospheric aerosol profiling, Atmos. Meas. Tech., 9, 1261–1277, https://doi.org/10.5194/amt-9-1261-2016,
535   publisher: Copernicus GmbH, 2016.

Emde, C. and Mayer, B.: Simulation of solar radiation during a total eclipse: a challenge for radiative transfer, Atmospheric Chem-
       istry and Physics, 7, 2259–2270, https://doi.org/https://doi.org/10.5194/acp-7-2259-2007, https://acp.copernicus.org/articles/7/2259/2007/
       acp-7-2259-2007.html, publisher: Copernicus GmbH, 2007.

Emde, C., Buras, R., Mayer, B., and Blumthaler, M.: The impact of aerosols on polarized sky radiance: model development, validation,
540   and applications, Atmospheric Chemistry and Physics, 10, 383–396, https://doi.org/https://doi.org/10.5194/acp-10-383-2010, https://acp.
       copernicus.org/articles/10/383/2010/acp-10-383-2010.html, publisher: Copernicus GmbH, 2010.

Emde, C., Buras, R., and Mayer, B.: ALIS: An efficient method to compute high spectral resolution polarized solar radiances using the Monte
       Carlo approach, Journal of Quantitative Spectroscopy and Radiative Transfer, 112, 1622–1631, https://doi.org/10.1016/j.jqsrt.2011.03.018,
       http://www.sciencedirect.com/science/article/pii/S0022407311001373, 2011.

545   Emde, C., Barlakas, V., Cornet, C., Evans, F., Korkin, S., Ota, Y., Labonnote, L. C., Lyapustin, A., Macke, A., Mayer, B., and Wendisch, M.:
       IPRT polarized radiative transfer model intercomparison project – Phase A, Journal of Quantitative Spectroscopy and Radiative Transfer,
       164, 8–36, https://doi.org/10.1016/j.jqsrt.2015.05.007, https://linkinghub.elsevier.com/retrieve/pii/S0022407315001922, 2015.

Emde, C., Buras-Schnell, R., Kylling, A., Mayer, B., Gasteiger, J., Hamann, U., Kylling, J., Richter, B., Pause, C., Dowling, T., and Bugliaro,
       L.: The libRadtran software package for radiative transfer calculations (version 2.0.1), Geoscientific Model Development, 9, 1647–1672,
550   https://doi.org/10.5194/gmd-9-1647-2016, https://www.geosci-model-dev.net/9/1647/2016/, 2016.

Emde, C., Buras-Schnell, R., Sterzik, M., and Bagnulo, S.: Influence of aerosols, clouds, and sunglint on polarization spectra of Earth-
       shine, Astronomy & Astrophysics, 605, A2, https://doi.org/10.1051/0004-6361/201629948, https://www.aanda.org/articles/aa/abs/2017/
       09/aa29948-16/aa29948-16.html, publisher: EDP Sciences, 2017.

Emde, C., Barlakas, V., Cornet, C., Evans, F., Wang, Z., Labonotte, L. C., Macke, A., Mayer, B., and Wendisch, M.: IPRT polar-
555   ized radiative transfer model intercomparison project – Three-dimensional test cases (phase B), Journal of Quantitative Spectroscopy
       and Radiative Transfer, 209, 19–44, https://doi.org/10.1016/J.JQSRT.2018.01.024, https://www.sciencedirect.com/science/article/pii/
       S0022407317308981, publisher: Pergamon, 2018.

Atmospheric
Measurement
Techniques
Discussions
Open Access
EGU

Flynn, L. E., Seftor, C. J., Larsen, J. C., and Xu, P.: The ozone mapping and profiler suite, in: Earth science satellite remote sensing, pp. 279–296, Springer, 2006.

560 Fussen, D., Baker, N., Debosscher, J., Dekemper, E., Demoulin, P., Errera, Q., Franssens, G., Mateshvili, N., Pereira, N., Pieroux, D., and Vanhellemont, F.: The ALTIUS atmospheric limb sounder, Journal of Quantitative Spectroscopy and Radiative Transfer, 238, 106 542, https://doi.org/10.1016/j.jqsrt.2019.06.021, http://www.sciencedirect.com/science/article/pii/S002240731930086X, 2019.

Herman, B. M., Ben-David, A., and Thome, K. J.: Numerical technique for solving the radiative transfer equation for a spherical shell atmosphere, Applied Optics, 33, 1760–1770, https://doi.org/10.1364/AO.33.001760, https://www.osapublishing.org/ao/abstract.cfm?uri=

565 ao-33-9-1760, publisher: Optical Society of America, 1994.

Herman, B. M., Caudill, T. R., Flittner, D. E., Thome, K. J., and Ben-David, A.: Comparison of the Gauss–Seidel spherical polarized radiative transfer code with other radiative transfer codes, Applied Optics, 34, 4563–4572, https://doi.org/10.1364/AO.34.004563, https://www.osapublishing.org/ao/abstract.cfm?uri=ao-34-21-4563, publisher: Optical Society of America, 1995.

Hovenier, J. W., Mee, C. V. M. v. d., and Domke, H.: Transfer of Polarized Light in Planetary Atmospheres: Basic Concepts and

570 Practical Methods, Astrophysics and Space Science Library, Springer Netherlands, https://doi.org/10.1007/978-1-4020-2856-4, https://www.springer.com/gp/book/9781402028557, 2004.

Kokhanovsky, A. A., Budak, V. P., Cornet, C., Duan, M., Emde, C., Katsev, I. L., Klyukov, D. A., Korkin, S. V., C-Labonnote, L., Mayer, B., Min, Q., Nakajima, T., Ota, Y., Prikhach, A. S., Rozanov, V. V., Yokota, T., and Zege, E. P.: Benchmark results in vector atmospheric radiative transfer, Journal of Quantitative Spectroscopy and Radiative Transfer, 111, 1931–1946, https://doi.org/10.1016/j.jqsrt.2010.03.005,

575 http://www.sciencedirect.com/science/article/pii/S0022407310000919, 2010.

Korkin, S., Yang, E.-S., Spurr, R., Emde, C., Krotkov, N., Vasilkov, A., Haffner, D., Mok, J., and Lyapustin, A.: Revised and extended benchmark results for Rayleigh scattering of sunlight in spherical atmospheres, Journal of Quantitative Spectroscopy and Radiative Transfer, 254, 107 181, https://doi.org/10.1016/j.jqsrt.2020.107181, http://www.sciencedirect.com/science/article/pii/S0022407320303976, 2020.

Kozun, M., Bourassa, A., Degenstein, D., and Loewen, P.: A multi-spectral polarimetric imager for atmospheric profiling of aerosol and

580 thin cloud: Prototype design and sub-orbital performance, Review of Scientific Instruments, https://doi.org/10.1063/5.0016129, accepted, 2020.

Kyrölä, E., Tamminen, J., Leppelmeier, G. W., Sofieva, V., Hassinen, S., Bertaux, J. L., Hauchecorne, A., Dalaudier, F., Cot, C., Korablev, O., Fanton d'Andon, O., Barrot, G., Mangin, A., Théodore, B., Guirlet, M., Etanchaud, F., Snoeij, P., Koopman, R., Saavedra, L., Fraisse, R., Fussen, D., and Vanhellemont, F.: GOMOS on Envisat: An overview, Advances in

585 Space Research, 33, 1020–1028, https://doi.org/10.1016/S0273-1177(03)00590-8, https://www.sciencedirect.com/science/article/pii/S0273117703005908, publisher: Pergamon, 2004.

Llewellyn, E. J., Lloyd, N. D., Degenstein, D. A., Gattinger, R. L., Petalina, S. V., Bourassa, A. E., Wiensz, J. T., Ivanov, E. V., McDade, I. C., Solheim, B. H., McConnell, J. C., Haley, C. S., Savigny, C. v., Sioris, C. E., McLinden, C. A., Griffioen, E., Kaminski, J., Evans, W. F. J., Puckrin, E., Strong, K., Wehrle, V., Hum, R. H., Kendall, D. J. W., Matsushita, J., Murtagh, D. P., Brohede, S., Stegman, J., Witt, G.,

590 Barnes, G., Payne, W. F., Piche, L., Smith, K., Warshaw, G., Deslauniers, D. L., Marchand, P., Richardson, E. H., King, R. A., Wevers, I., McCreath, W., Kyrölä, E., Oikarinen, L., Leppelmeier, G. W., Auvinen, H., Megle, G., Hauchecorne, A., Lefevre, F., de La Noe, J., Ricaud, P., Frisk, U., Sjoberg, F., Scheele, F. v., and Nordh, L.: The OSIRIS instrument on the Odin spacecraft, Canadian Journal of Physics, 82:6, s. 4, 411–422, 2004.

Atmospheric
Measurement
Techniques
Discussions

Open Access
EGU

Loughman, R., Flittner, D., Nyaku, E., and Bhartia, P. K.: Gauss–Seidel limb scattering (GSLS) radiative transfer model development in support of the Ozone Mapping and Profiler Suite (OMPS) limb profiler mission, Atmospheric Chemistry and Physics, 15, 3007–3020, https://doi.org/10.5194/acp-15-3007-2015, http://www.atmos-chem-phys.net/15/3007/2015/, 2015.

Loughman, R. P., Griffioen, E., Oikarinen, L., Postylyakov, O. V., Rozanov, A., Flittner, D. E., and Rault, D. F.: Comparison of radiative transfer models for limb-viewing scattered sunlight measurements, Journal of Geophysical Research: Atmospheres, 109, n/a–n/a, https://doi.org/10.1029/2003JD003854, http://doi.wiley.com/10.1029/2003JD003854, iSBN: 0148-0227, 2004.

Loughman, R. P., Flittner, D. E., Herman, B. M., Bhartia, P. K., Hilsenrath, E., and McPeters, R. D.: Description and sensitivity analysis of a limb scattering ozone retrieval algorithm, Journal of Geophysical Research, 110, D19 301, https://doi.org/10.1029/2004JD005429, http://doi.wiley.com/10.1029/2004JD005429, 2005.

Malicet, J., Daumont, D., Charbonnier, J., Parisse, C., Chakir, A., and Brion, J.: Ozone UV spectroscopy. II. Absorption cross-sections and temperature dependence, Journal of atmospheric chemistry, 21, 263–273, publisher: Springer, 1995.

Malinina, E., Rozanov, A., Rozanov, V., Liebing, P., Bovensmann, H., and Burrows, J. P.: Aerosol particle size distribution in the stratosphere retrieved from SCIAMACHY limb measurements, Atmospheric Measurement Techniques, 11, 2085–2100, https://doi.org/https://doi.org/10.5194/amt-11-2085-2018, https://amt.copernicus.org/articles/11/2085/2018/, publisher: Copernicus GmbH, 2018.

Malinina, E., Rozanov, A., Rieger, L., Bourassa, A., Bovensmann, H., Burrows, J. P., and Degenstein, D.: Stratospheric aerosol characteristics from space-borne observations: extinction coefficient and Ångström exponent, Atmospheric Measurement Techniques, 12, 3485–3502, https://doi.org/https://doi.org/10.5194/amt-12-3485-2019, https://amt.copernicus.org/articles/12/3485/2019/, publisher: Copernicus GmbH, 2019.

Malinina, E., Rozanov, A., Niemeier, U., Peglow, S., Arosio, C., Wrana, F., Timmreck, C., von Savigny, C., and Burrows, J. P.: Changes in stratospheric aerosol extinction coefficient after the 2018 Ambae eruption as seen by OMPS-LP and ECHAM5-HAM, Atmospheric Chemistry and Physics Discussions, pp. 1–25, https://doi.org/https://doi.org/10.5194/acp-2020-749, https://acp.copernicus.org/preprints/acp-2020-749/, publisher: Copernicus GmbH, 2020.

Marchuk, G. I., Mikhailov, G. A., Nazareliev, M., Darbinjan, R. A., Kargin, B. A., and Elepov, B. S.: The Monte Carlo methods in atmospheric optics, vol. 12, Springer, 2013.

Mauldin, L. E., Salikhov, R., Habib, S., Vladimirov, A. G., Carraway, D., Petrenko, G., and Comella, J.: Meteor-3M(1)/Stratospheric Aerosol and Gas Experiment III (SAGE III) jointly sponsored by the National Aeronautics and Space Administration and the Russian Space Agency, p. 355, International Society for Optics and Photonics, https://doi.org/10.1117/12.317767, http://proceedings.spiedigitallibrary.org/proceeding.aspx?doi=10.1117/12.317767, 1998.

Mayer, B.: Radiative transfer in the cloudy atmosphere, EPJ Web of Conferences, 1, 75–99, https://doi.org/10.1140/epjconf/e2009-00912-1, https://www.epj-conferences.org/articles/epjconf/abs/2009/01/epjconf1008/epjconf1008.html, publisher: EDP Sciences, 2009.

Mayer, B. and Kylling, A.: Technical note: The libRadtran software package for radiative transfer calculations - description and examples of use, Atmospheric Chemistry and Physics, 5, 1855–1877, https://doi.org/10.5194/acp-5-1855-2005, http://www.atmos-chem-phys.net/5/1855/2005/, 2005.

McLinden, C. A. and Bourassa, A. E.: A Systematic Error in Plane-Parallel Radiative Transfer Calculations, Journal of the Atmospheric Sciences, 67, 1695–1699, https://doi.org/10.1175/2009JAS3322.1, 2010.

630   Mishchenko, M. I., Lacis, A. A., and Travis, L. D.: Errors induced by the neglect of polarization in radiance calculations for rayleigh-scattering atmospheres, Journal of Quantitative Spectroscopy and Radiative Transfer, 51, 491–510, https://doi.org/10.1016/0022-4073(94)90149-X, http://www.sciencedirect.com/science/article/pii/002240739490149X, 1994.

Murtagh, D., Frisk, U., Merino, F., Ridal, M., Jonsson, A., Stegman, J., Witt, G., Jiménez, C., Megie, G., Noë, J. D., Ricaud, P., Baron, P., Pardo, J. R., Llewellyn, E. J., Degenstein, D. A., Gattinger, R. L., Lloyd, N. D., Evans, W. F. J., McDade, I. C., Haley, C. S., Sioris, C. E.,

635   Savigny, V., Solheim, B. H., McConnell, J. C., Richardson, E. H., Leppelmeier, G. W., Auvinen, H., and Oikarinen, L.: An overview of the Odin atmospheric mission, Canadian Journal of Physics, 80, 309–318, https://doi.org/10.1139/P01-157, 2002.

Natraj, V. and Hovenier, J.: Polarized light reflected and transmitted by thick Rayleigh scattering atmospheres, The Astrophysical Journal, 748, 28, publisher: IOP Publishing, 2012.

Oikarinen, L.: Polarization of light in UV-visible limb radiance measurements, Journal of Geophysical Research: Atmospheres, 106,

640   1533–1544, https://doi.org/10.1029/2000JD900442, https://agupubs.onlinelibrary.wiley.com/doi/abs/10.1029/2000JD900442, _eprint: https://agupubs.onlinelibrary.wiley.com/doi/pdf/10.1029/2000JD900442, 2001.

Oikarinen, L.: Effect of surface albedo variations on UV-visible limb-scattering measurements of the atmosphere, Journal of Geophysical Research: Atmospheres, 107, ACH 13–1–ACH 13–15, https://doi.org/10.1029/2001JD001492, https://agupubs.onlinelibrary.wiley.com/doi/abs/10.1029/2001JD001492, _eprint: https://agupubs.onlinelibrary.wiley.com/doi/pdf/10.1029/2001JD001492, 2002.

645   Oikarinen, L., Sihvola, E., and Kyrölä, E.: Multiple scattering radiance in limb-viewing geometry, Journal of geophysical research, 104, 1999.

Palmer, K. F. and Williams, D.: Optical Constants of Sulfuric Acid; Application to the Clouds of Venus?, Applied Optics, 14, 208–219, https://doi.org/10.1364/AO.14.000208, https://www.osapublishing.org/ao/abstract.cfm?uri=ao-14-1-208, publisher: Optical Society of America, 1975.

650   Postylyakov, O.: Linearized vector radiative transfer model MCC++ for a spherical atmosphere, Journal of Quantitative Spectroscopy and Radiative Transfer, 88, 297–317, https://doi.org/10.1016/j.jqsrt.2004.01.009, 2004.

Ramon, D., Steinmetz, F., Jolivet, D., Compiègne, M., and Frouin, R.: Modeling polarized radiative transfer in the ocean-atmosphere system with the GPU-accelerated SMART-G Monte Carlo code, Journal of Quantitative Spectroscopy and Radiative Transfer, 222-223, 89–107, https://doi.org/10.1016/j.jqsrt.2018.10.017, http://www.sciencedirect.com/science/article/pii/S002240731830400X, 2019.

655   Rault, D. F.: Ozone profile retrieval from Stratospheric Aerosol and Gas Experiment (SAGE III) limb scatter measurements, Journal of Geophysical Research, 110, D09 309, https://doi.org/10.1029/2004JD004970, http://doi.wiley.com/10.1029/2004JD004970, 2005.

Rault, D. F. and Loughman, R. P.: The OMPS Limb Profiler Environmental Data Record Algorithm Theoretical Basis Document and Expected Performance, IEEE Transactions on Geoscience and Remote Sensing, 51, 2505–2527, https://doi.org/10.1109/TGRS.2012.2213093, http://ieeexplore.ieee.org/document/6329422/, 2013.

660   Rault, D. F. and Spurr, R.: The OMPS Limb Profiler instrument: two-dimensional retrieval algorithm, in: Remote Sensing, pp. 78 270P–78 270P, International Society for Optics and Photonics, 2010.

Rieger, L. A., Malinina, E. P., Rozanov, A. V., Burrows, J. P., Bourassa, A. E., and Degenstein, D. A.: A study of the approaches used to retrieve aerosol extinction, as applied to limb observations made by OSIRIS and SCIAMACHY, Atmospheric Measurement Techniques, 11, 3433–3445, https://doi.org/10.5194/amt-11-3433-2018, https://www.atmos-meas-tech.net/11/3433/2018/, 2018.

665   Rieger, L. A., Zawada, D. J., Bourassa, A. E., and Degenstein, D. A.: A Multiwavelength Retrieval Approach for Improved OSIRIS Aerosol Extinction Retrievals, Journal of Geophysical Research: Atmospheres, 124, 7286–7307,

https://doi.org/10.1029/2018JD029897, https://agupubs.onlinelibrary.wiley.com/doi/abs/10.1029/2018JD029897, _eprint: https://agupubs.onlinelibrary.wiley.com/doi/pdf/10.1029/2018JD029897, 2019.

Roth, C. Z., Degenstein, D. A., Bourassa, A. E., and Llewellyn, E. J.: The retrieval of vertical profiles of the ozone number density using
670   Chappuis band absorption information and a multiplicative algebraic reconstruction technique, Canadian Journal of Physics, 85, 1225–
1243, https://doi.org/10.1139/p07-130, https://www.nrcresearchpress.com/doi/10.1139/P07-130, publisher: NRC Research Press, 2007.

Rozanov, A., Rozanov, V., and Burrows, J. P.: A numerical radiative transfer model for a spherical planetary atmosphere: combined differen-
tial–integral approach involving the Picard iterative approximation, Journal of Quantitative Spectroscopy and Radiative Transfer, 69, 491–
512, https://doi.org/10.1016/S0022-4073(00)00100-X, http://www.sciencedirect.com/science/article/pii/S002240730000100X, 2001.

675 Rozanov, A., Eichmann, K.-U., von Savigny, C., Bovensmann, H., Burrows, J. P., von Bargen, A., Doicu, A., Hilgers, S., Godin-
Beekmann, S., Leblanc, T., and McDermid, I. S.: Comparison of the inversion algorithms applied to the ozone vertical profile re-
trieval from SCIAMACHY limb measurements, Atmos. Chem. Phys., 7, 4763–4779, https://doi.org/10.5194/acp-7-4763-2007, http:
//www.atmos-chem-phys.net/7/4763/2007/, publisher: Copernicus GmbH, 2007.

Rozanov, A., Kühl, S., Doicu, A., McLinden, C., Puķīte, J., Bovensmann, H., Burrows, J. P., Deutschmann, T., Dorf, M., Goutail, F., Grunow,
680   K., Hendrick, F., von Hobe, M., Hrechanyy, S., Lichtenberg, G., Pfeilsticker, K., Pommereau, J. P., Van Roozendael, M., Stroh, F., and Wag-
ner, T.: BrO vertical distributions from SCIAMACHY limb measurements: comparison of algorithms and retrieval results, Atmospheric
Measurement Techniques, 4, 1319–1359, https://doi.org/https://doi.org/10.5194/amt-4-1319-2011, https://amt.copernicus.org/articles/4/
1319/2011/, publisher: Copernicus GmbH, 2011a.

Rozanov, A., Weigel, K., Bovensmann, H., Dhomse, S., Eichmann, K. U., Kivi, R., Rozanov, V., Vömel, H., Weber, M., and Burrows, J. P.:
685   Retrieval of water vapor vertical distributions in the upper troposphere and the lower stratosphere from SCIAMACHY limb measurements,
Atmos. Meas. Tech., 4, 933–954, https://doi.org/10.5194/amt-4-933-2011, publisher: Copernicus GmbH, 2011b.

Rozanov, V., Rozanov, A., Kokhanovsky, A., and Burrows, J.: Radiative transfer through terrestrial atmosphere and ocean: Software package
SCIATRAN, Journal of Quantitative Spectroscopy and Radiative Transfer, 133, 13–71, https://doi.org/10.1016/J.JQSRT.2013.07.004,
https://www.sciencedirect.com/science/article/pii/S0022407313002872, publisher: Pergamon, 2014.

690 Sioris, C. E., Rieger, L. A., Lloyd, N. D., Bourassa, A. E., Roth, C. Z., Degenstein, D. A., Camy-Peyret, C., Pfeilsticker, K., Berthet, G.,
Catoire, V., Goutail, F., Pommereau, J. P., and McLinden, C. A.: Improved OSIRIS NO2 retrieval algorithm: Description and validation,
Atmospheric Measurement Techniques, 10, 1155–1168, https://doi.org/10.5194/amt-10-1155-2017, https://www.atmos-meas-tech.net/10/
1155/2017/, 2017.

Taha, G., Rault, D. F., Loughman, R. P., Bourassa, A. E., and Von Savigny, C.: SCIAMACHY stratospheric aerosol extinction profile retrieval
695   using the OMPS/LP algorithm, Atmospheric Measurement Techniques, 4, 547–556, https://doi.org/10.5194/amt-4-547-2011, publisher:
Copernicus GmbH, 2011.

Taha, G., Loughman, R., Zhu, T., Thomason, L., Kar, J., Rieger, L., and Bourassa, A.: OMPS LP Version 2.0 Multi-
wavelength Aerosol Extinction Coefficient Retrieval Algorithm, Atmospheric Measurement Techniques Discussions, pp. 1–34,
https://doi.org/https://doi.org/10.5194/amt-2020-329, https://amt.copernicus.org/preprints/amt-2020-329/, publisher: Copernicus GmbH,
700   2020.

Thomason, L. W., Ernest, N., Millán, L., Rieger, L., Bourassa, A., Vernier, J.-P., Manney, G., Luo, B., Arfeuille, F., and
Peter, T.: A global space-based stratospheric aerosol climatology: 1979–2016, Earth System Science Data, 10, 469–492,
https://doi.org/https://doi.org/10.5194/essd-10-469-2018, https://essd.copernicus.org/articles/10/469/2018/, publisher: Copernicus GmbH,
2018.

705 Von Savigny, C., Ernst, F., Rozanov, A., Hommel, R., Eichmann, K. U., Rozanov, V., Burrows, J. P., and Thomason, L. W.: Improved
       stratospheric aerosol extinction profiles from SCIAMACHY: Validation and sample results, Atmospheric Measurement Techniques, 8,
       5223–5235, https://doi.org/10.5194/amt-8-5223-2015, publisher: Copernicus GmbH, 2015.

Waters, J. W., Froidevaux, L., Harwood, R. S., Jarnot, R. F., Pickett, H. M., Read, W. G., Siegel, P. H., Cofield, R. E., Filipiak, M. J., Flower,
       D. A., Holden, J. R., Lau, G. K., Livesey, N. J., Manney, G. L., Pumphrey, H. C., Santee, M. L., Wu, D. L., Cuddy, D. T., Lay, R. R., Loo,
710   M. S., Perun, V. S., Schwartz, M. J., Stek, P. C., Thurstans, R. P., Boyles, M. A., Chandra, K. M., Chavez, M. C., Chen, G. S., Chudasama,
       B. V., Dodge, R., Fuller, R. A., Girard, M. A., Jiang, J. H., Jiang, Y., Knosp, B. W., Labelle, R. C., Lam, J. C., Lee, K. A., Miller, D.,
       Oswald, J. E., Patel, N. C., Pukala, D. M., Quintero, O., Scaff, D. M., Van Snyder, W., Tope, M. C., Wagner, P. A., and Walch, M. J.:
       The Earth Observing System Microwave Limb Sounder (EOS MLS) on the aura satellite, IEEE Transactions on Geoscience and Remote
       Sensing, 44, 1075–1092, https://doi.org/10.1109/TGRS.2006.873771, iSBN: 0196-2892, 2006.

715 Wiscombe, W. J.: Improved Mie scattering algorithms., Applied optics, 19, 1505–9, 1980.

Zawada, D., Franssens, G., Loughman, R., Mikkonen, A., Rozanov, A., Emde, C., Bourassa, A., Dueck, S., Lindqvist, H., Ramon, D.,
       Rozanov, V., Dekemper, E., Kyrölä, E., Burrows, J. P., Fussen, D., and Degenstein, D.: Radiance data for "Systematic Comparison of
       Vectorial Spherical Radiative Transfer Models in Limb Scattering Geometry" by Zawada et al., https://doi.org/10.5281/zenodo.4292303,
       https://doi.org/10.5281/zenodo.4292303, 2020.

720 Zawada, D. J., Dueck, S. R., Rieger, L. A., Bourassa, A. E., Lloyd, N. D., and Degenstein, D. A.: High-resolution and Monte Carlo additions
       to the SASKTRAN radiative transfer model, Atmos. Meas. Tech., 8, 2609–2623, https://doi.org/10.5194/amt-8-2609-2015, http://www.
       atmos-meas-tech.net/8/2609/2015/amt-8-2609-2015.html, publisher: Copernicus GmbH, 2015.

Zawada, D. J., Rieger, L. A., Bourassa, A. E., and Degenstein, D. A.: Tomographic retrievals of ozone with the OMPS Limb Profiler:
       algorithm description and preliminary results, Atmospheric Measurement Techniques, 11, 2375–2393, https://doi.org/10.5194/amt-11-
725   2375-2018, https://www.atmos-meas-tech.net/11/2375/2018/, 2018.